https://doi.org/10.5194/egusphere-2022-961
Preprint. Discussion started: 1 November 2022

Modeling global wildfire activity in the intermediate complexity University of Victoria Earth System Climate Model (UVic ESCM 2.9) : the importance of the simulated climatology

Étienne Guertin[1] and H. Damon Matthews[1]

[1]Department of Geography, Planning and Environment, Concordia University, Montréal, QC, Canada

Correspondence: Étienne Guertin (etienne.guertin@mail.concordia.ca)

Abstract. Fire is an integral part of the Earth system, interacting in complex ways with humans, vegetation and climate. Global fire activity is an important element of the carbon cycle, and understanding its role in the context of climate change is crucial. In order to represent the transient fire-climate-vegetation interactions and to integrate these in the long term climate projections of climate models, coupling these three components is necessary. Global fire models have been coupled to climate-vegetation models with complex atmosphere modules but these models are computationally intensive. In this research, we use the University of Victoria Earth System Climate Model 2.9 (UVic ESCM), an ESCM of intermediate complexity to which we couple a process based global fire model, in order to develop a computationally efficient means of studying long term fire-climate-vegetation interactions. The fire model used simulates burned area based primarily on relative humidity, soil moisture and biomass density. The UViC ESCM's simulated relative humidity is improved by parameterizing it according to the simulated precipitation, and observational variability is added to the simulated climatology to improve the variability of simulated burned area. The best parameterization achieves a moderate spatial agreement of simulated burned area with observational data. Tropical rainforests in South America and Africa, however, display very high burned fractions, due to the poorly simulated relative humidity input; indeed, when we used observed relative humidity to simulate fire activity, the pattern of burned area in the tropics improved substantially. This research demonstrates the importance of variability and regional patterns of climatology for global wildfire activity and the corresponding limitations of ESCMs that simplify atmospheric circulation. This suggests that using pattern scaling of climate variables as an input to fire models could provide such ESCMs of intermediate complexity with the ability to integrate global fire activity.

1 Introduction

1.1 Importance in the Earth System

Fire is a crucial component of the global carbon cycle via its interaction with global vegetation distribution and structure, and is deeply intertwined with climatic and weather conditions and anthropogenic activities (Bowman et al., 2009). About 3% of global vegetated land surface burns annually (Giglio et al., 2013; Ding et al., 2020), generating fire-caused carbon emissions (i.e. gross carbon emissions to the atmosphere due to fire, including deforestation fires) equivalent to 20% of anthropogenic

https://doi.org/10.5194/egusphere-2022-961
Preprint. Discussion started: 1 November 2022

CO_2 emissions (Yang et al., 2015; Van der Werf et al., 2010). The net CO_2 effect of burning biomass on the climate, however, differs from the effect of CO_2 emissions from fossil fuel burning, because of vegetation regrowth and decomposition (Landry and Matthews, 2016) and long term carbon sequestration in pyrogenic carbon (Landry and Matthews, 2017; Jones et al., 2019). Through these processes, between 50%-80% of 20th century fire-caused carbon emissions have returned to the terrestrial carbon pool (Li et al., 2014; Yue et al., 2014; Yang et al., 2015). Global fire activity also significantly contributes to other greenhouse gas (Van der Werf et al., 2010; Ciais et al., 2013) and aerosol (Andreae and Merlet, 2001) with aerosol cooling effects (Ward et al., 2012) emissions and to land surface albedo changes (Landry and Matthews, 2016). Driven by climate change, long fire weather season now affects significantly more fire-susceptible land globally and occurs much more frequently (Jolly et al., 2015). End-of-century projections generally agree that global yearly burned area and fire-caused emissions will increase with warming (Moritz et al., 2012; Kloster et al., 2012; Pechony and Shindell, 2010). Fire could have a small but non-negligible warming (Tosca et al., 2013; Knorr et al., 2015) or a greater cooling (Ward et al., 2012; Landry et al., 2015) feedback on the climate.

Global burned area datasets derived from satellite observations in the past 25 years have allowed to identify the drivers of fire activity for finer spatial and temporal scales (e.g. Bistinas et al., 2014; Kelley et al., 2019), and to develop process-based models with varying levels of complexity which, when coupled to Dynamic Global Vegetation Models (DGVMs), are able to represent the observed patterns and trends and identify and quantify feedbacks between fire, vegetation and climate (Hantson et al., 2016). The Fire Model Intercomparison Project (FireMIP) has assessed, for several benchmarks, state-of-the-art global fire-vegetation models with varying levels of complexity, parameterization and structure (Hantson et al., 2016, Hantson et al., 2020). Some of these fire-vegetation models have been coupled to climate models and used in the Climate Model Intercomparison Project 6 (CMIP6) to assess global fire-caused carbon emissions under different climate change scenarios (Kasoar et al., 2021). The atmospheric modules of these coupled fire-vegetation-climate models are General Circulation Models (GCMs), which largely contribute to making CMIP6 simulations computationally intensive.

However, Earth system Models of Intermediate Complexity (EMIC; Claussen et al., 2002) offer a more computationally efficient approach to simulate century-scale Earth system dynamics. Many EMICs have a simplified atmosphere component coupled to comprehensive representations of the carbon cycle and of ocean circulation, which allows them to simulate century-scale temperature responses to greenhouse gas emission scenarios at a relatively low computation cost (e.g. a few days at most using a common desktop computer; Mengis et al., 2020). To the best of our knowledge and despite the potential importance of fire for long term temperature projections, there currently exists only one EMIC with an interactive fire model (see Wu et al., 2021). Fire activity patterns are highly sensitive to fire weather conditions, and thus it is not clear to which degree it is possible to simplify the representation of atmospheric processes without sacrificing the main patterns of global fire activity.

In this study, we address the absence of interactive fire models coupled to EMICs by coupling a process-based fire model to the University of Victoria Earth System Climate Model (UVic ESCM, Weaver et al., 2001). The UVic ESCM has been used to demonstrate the irreversibility of CO_2-induced warming (Matthews and Caldeira, 2008; Eby et al., 2009) and the proportionality of emissions to global temperature change (Matthews et al., 2009; Zickfeld et al., 2009) and has also been included in the sixth phase of the Coupled Model Intercomparison Project (CMIP6). The goal of this study is to simulate the

https://doi.org/10.5194/egusphere-2022-961
Preprint. Discussion started: 1 November 2022

spatial patterns of fire in an EMIC so as to allow the study of fire-climate-vegetation interactions in the context of climate change.

In the following sections, we first summarize the various components of the model we used and how they are coupled. We then describe how we modified the UVic ESCM's climatology and the fire model to improve their coupling. We follow with the main results offered by the coupled model and then discuss the limitations of this approach and possible improvements toward a more viable approach.

2 Methods

2.1 UVic ESCM

The UVic-ESCM (Weaver et al., 2001) is a 3.6° X 1.8° Earth system Model of Intermediate Complexity (EMIC) (Claussen et al., 2002). EMICs are well suited to predict long-term temperature change and the interaction of various components of the ocean, land and atmosphere over this time period (Claussen et al., 2002). The UVic ESCM contains a 19 layer ocean general circulation model coupled to a thermodynamic/dynamic sea-ice model, a single layer thermo-mechanical land ice model and a single layer reduced complexity vertically integrated energy-moisture balance atmospheric model. All modules are coupled together every 5 model days and the simulated climate variables exhibit variability at a monthly timestep. Present-day winds are prescribed in the atmosphere model and a dynamical wind feedback is added to allow a first order approximation of wind stress changes in a changing climate. Precipitation occurs when relative humidity reaches 85%. Simulated globally-averaged annual precipitation is in good agreement with observations, but the agreement is less able to accurately simulate spatial patterns and temporal variability (Mengis et al., 2020).

2.2 MOSES-TRIFFID land surface - vegetation modules

The UVic ESCM is coupled to a land surface scheme (Meissner et al., 2003), a simplified version of the Met Office Surface Exchange Scheme (MOSES); and a Dynamic Global Vegetation Model (DGVM), the Top-down Representation of Interactive Foliage and Flora Including Dynamics (TRIFFID) (Cox, 2001). The MOSES is a single layer which describes the land module in terms of lying snow, skin and soil temperature and soil moisture content. TRIFFID explicitly models five plant functional types (PFT): broadleaf trees, needleleaf trees, C3 grasses, C4 grasses and shrubs, which are recognized by MOSES. Inputs from the climate module influence vegetation structure, distribution and growth, which change land-surface parameters and affect atmospheric CO_2 concentration. The areal coverage, leaf area index and canopy height of each PFT are calculated for each grid cell based on carbon availability in the land surface scheme and a Lotka-Volterra competition model. Carbon fluxes, the difference between photosynthesis and plant respiration, depend both on climate and atmospheric CO_2 concentration. Carbon is transferred to the soil in the land surface scheme by litterfall. From the soil, carbon is transferred to the atmosphere by microbial respiration, which depends on soil moisture and temperature. Carbon and water fluxes are coupled with the atmosphere every five days, and with the TRIFFID DGVM every month. The TRIFFID model then passes vegetation information to the land

https://doi.org/10.5194/egusphere-2022-961
Preprint. Discussion started: 1 November 2022

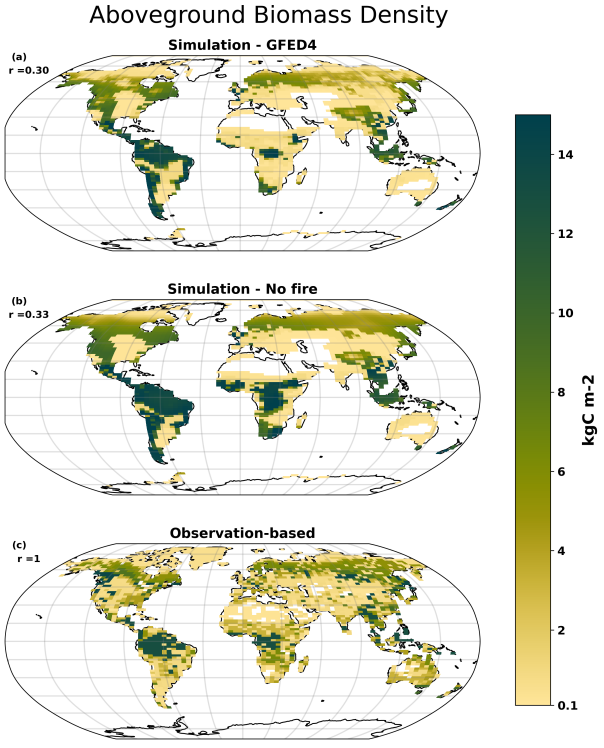

Figure 1. Aboveground vegetation carbon density, simulated using prescribed GFED4 burned area, simulated without fire and observed. Observed data from Spawn et al. (2020).

surface scheme which updates its vegetation-dependent parameters. The TRIFFID explicitly describes vegetation in detail but it is less complex than other DGVMs in terms of PFT diversity. For example, the Community Land Model (CLM; Levis et al., 2004) used in fire modeling by Li et al. (2012b) and Kloster et al. (2010) has 10 PFTs instead of the 5 PFTs of TRIFFID in the UVic ESCM. The simulated vegetation structure (the proportion of each PFT per gridcell) is spatially correlated with observations at r=0.635 (Meissner et al., 2003), which is comparable to when TRIFFID has been coupled to atmospheric general circulation models. However, specific areas show low correlation due to complex physiological responses not captured by global vegetation models and because of climate biases simulated by the UVic ESCM. Moreover, vegetation carbon density ($\mathrm{kgCm^{-2}}$) per gridcell, an important driver of fire activity, correlates moderately well with observations at r=0.33 (Fig. 1**b**) in a simulation with the default biomass mortality parameterization (constant loss rate attributed to disturbance independent of climate and vegetation), and r=0.30 (Fig.1**a**) with prescribed burned area dataset from observations (GFED4, Giglio et al., 2013).

https://doi.org/10.5194/egusphere-2022-961
Preprint. Discussion started: 1 November 2022

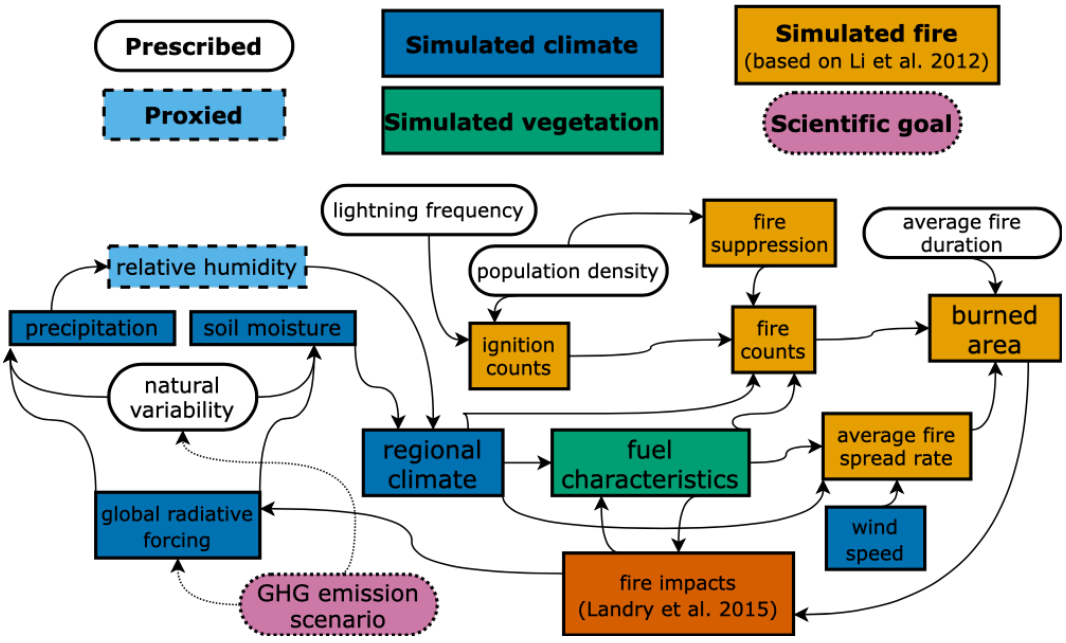

Figure 2. Fire parameterization diagram of the present study. Dotted arrows represent a transient simulation using different GHG emission scenarios. The current study looks at an equilibrium climate scenario.

2.3 Fire parameterization

The fire parameterization used in this study models fire as a mechanistic process (Fig. 2; adapted from Li et al. (2012b)) with three mains steps: (1) fire occurrence (sect. 2.3.1), (2) fire spread (sect. 2.3.2) and (3) fire impacts (sect. 2.3.3). For steps (1) and (2), our parameterization draws from Li et al. (2012b) and for step (3) we use the parametrization by Landry et al. (2015). Our fire model calculates the number of ignitions per gridcell based on prescribed observed lightning frequency and population density, as ignitions that have the potential to lead to vegetation fires are both natural and anthropogenic. The agriculture fraction (crop + pasture) is prescribed in the UVic ESCM and is treated as if it were natural vegetation by the fire parameterization. The Li et al. (2012b) parameterization makes the same assumption. Based on ignition counts, anthropogenic fire suppression rates, climate variables (relative humidity and soil moisture) and vegetation characteristics (carbon density and PFT), fire counts are estimated. Average fire spread rate is also estimated based on simulated climate and vegetation variables. Combined with a prescribed average fire duration, average fire spread rate and fire counts are used to calculate burned area per grid cell. The fire impacts module calculates how much of this burned area remains alive after the fire and the resulting emissions impacts, based on the type of vegetation that burns. The following sects. 2.3.1-2.3.3 describe the fire model and the modifications brought to the UVic ESCM atmospheric module. The parameters used in the formulas are described in Table 1.

https://doi.org/10.5194/egusphere-2022-961
Preprint. Discussion started: 1 November 2022

2.3.1 Fire occurrence

The number of ignitions N_i in a grid cell is

$$N_i = I_n + I_a \tag{1}$$

where I_n is the number of natural ignitions and I_a the number of anthropogenic ignitions.

The number of natural ignitions is

$$I_n = I_l \cdot I_{ratio} \cdot \gamma \tag{2}$$

where I_l is the total number of lightning flashes, I_{ratio} is the ratio between the number of cloud-to-ground flashes and the number of lightning flashes and γ is the ignition efficiency of cloud-to-ground lightning (Latham and Schlieter, 1989).

I_{ratio} is given by

$$I_{ratio} = \frac{1}{5.16 + 2.16 \cdot cos(3 \cdot lat)} \tag{3}$$

where lat is the latitude in degrees (Prentice and Mackerras, 1977).

The number of anthropogenic ignitions I_a ($\mathrm{countmonth}^{-1}$) is

$$I_a = 0.026452 \cdot D^{0.4} \tag{4}$$

where D is the population density ($\mathrm{nopeoplekm}^{-2}$) (Li et al., 2012b).

Fire counts N_f ($i.e.$ the number of ignitions that start a fire) are

$$N_f = \begin{cases} 0 & \text{if } snow > 0. \\ N_i \cdot f_b \cdot f_m \cdot (1 - f_s) & \text{if } snow = 0. \end{cases} \tag{5}$$

where snow is the amount of lying snow, f_b is the fuel availability, f_m is the fuel combustibility and f_s is the fire anthropogenic suppression (Li et al., 2012b). The three f functions vary between 0 and 1.

Fuel availability f_b is a function of biomass surface density and is given by

$$f_b = \begin{cases} 0 & \text{if } B_{act} < B_{low}. \\ \frac{B_{act} - B_{low}}{B_{up} - B_{low}} & \text{if } B_{low} \leq B_{act} \leq B_{up}. \\ 1 & \text{if } B_{act} > B_{up}. \end{cases} \tag{6}$$

https://doi.org/10.5194/egusphere-2022-961
Preprint. Discussion started: 1 November 2022

where B_{act} is the actual biomass density ($\mathrm{gCm^{-2}}$), B_{low} is the minimum biomass density at which a fire can start and B_{up} is the biomass density over which fuel availability no longer limits ignitions from starting fires (Li et al., 2012b).

Fuel combustibility f_m is

$$f_m = f_{RH} \cdot f_\theta \tag{7}$$

where f_{RH} is a function of relative humidity (RH) and f_θ is a function of soil moisture (Li et al., 2012b). Both functions vary between 0 and 1.

f_{RH} is given by

$$f_{RH} = \begin{cases} 1 & \text{if } RH_{act} \leq RH_{low}. \\ \frac{RH_{high} - RH_{act}}{RH_{high} - RH_{low}} & \text{if } RH_{low} < RH < RH_{high}. \\ 0 & \text{if } RH_{act} \geq RH_{high}. \end{cases} \tag{8}$$

where RH_{act} is the actual relative humidity, RH_{low} is the RH below which ignitions are not limited by RH and RH_{high} is the maximum RH over which a fire cannot start.

f_θ is calculated from the soil moisture θ

$$f_\theta = e^{\left[-\pi\left(\frac{\theta}{\theta_e}\right)^2\right]} \tag{9}$$

where θ is the soil moisture (SM) relative to the saturation soil moisture SM_{SAT} and θ_e is the extinction coefficient of soil wetness (Li et al., 2012b). The choice of θ_e determines a threshold soil moisture level at which the success of ignitions is very small.

Fire suppression f_s by humans is a function of population density D and is applied to fire counts by the following relationship:

$$f_s = \epsilon_1 - \epsilon_2 \cdot e^{(-\alpha \cdot D)} \tag{10}$$

where ϵ_1 and ϵ_2 and α are constants (Li et al., 2012b; Pechony and Shindell, 2009).

2.3.2 Fire spread

In Li et al., 2012b, the average fire duration is assumed to be 1 day which is an underestimate of large scale wildfires which last many days. This value is still a good estimate of fire duration, as it corresponds to the mathematical expectation of an empirically-derived exponential distribution of fire duration (Venevsky et al., 2002).

https://doi.org/10.5194/egusphere-2022-961
Preprint. Discussion started: 1 November 2022

Fire parameter	Description	Value by model				Units
		Precip proxy ($rhsim$)	Prescribed RH ($rhobs$)	Base ($rhsimBase$)	Other literature	
γ	cloud-to-ground lightning ignition efficiency	0.04[6]	0.04[6]	0.25[1]		dmnl
θ_e	extinction coefficient of soil wetness	0.55[6]	0.69[2]	0.69[2]	0.3[4]/0.35[3]	dmnl
SM_{SAT}	saturated soil moisture	458[2]	458[2]	458[2]		kgm^{-2}
Θ_w	wilting soil moisture content	0.13[6]	0.13[6]	0.136[3]		dmnl
Θ_c	critical soil moisture content	0.34[6]	0.34[6]	0.242[3]		dmnl
$g(0)$	constant	0.05[2]	0.05[2]	0.05[2]		dmnl
B_{low}	min. biomass density for fuel availability	90[6]	90[6]	155[2]		gCm^{-2}
B_{up}	max. biomass density for fuel availability	1050[2]	1050[2]	1050[2]		gCm^{-2}
RH_{low}	min. relative humidity for fuel combustibility	0.3[2]	0.4[6]	0.3[2]		dmnl
RH_{high}	max. relative humidity for fuel combustibility	0.7[2]	0.9[6]	0.7[2]		dmnl
ε_1	fire suppression constant	0.99[2]	0.99[2]	0.99[2]	0.95[5]	dmnl
ε_2	fire suppression constant	0.98[2]	0.98[2]	0.98[2]	0.90[5]	dmnl
α	fire suppression constant	0.025[2]	0.025[2]	0.025[2]	0.05[5]	dmnl
u_{max}	maximum fire spread rate (BT/NT/S/C3/C4)	0.11/ 0.15/ 0.17/ 0.2/ 0.2 [2]				ms^{-1}
Ω	burned area factor	1[6]	2[6]	1[6]		dmnl
Climate parameter						
PR_{min}	min. precipitation threshold (RH_{sim})	1e-07[6]	na	1e-07[6]		mms^{-1}
PR_{max}	max. precipitation threshold (RH_{sim})	1e-05[6]	na	1e-05[6]		mms^{-1}

Table 1. Fire and climate parameters values used. Plant Function Types (PFTs) are Broadleaf trees (BT), needleleaf trees (NT), shrubs (S), C3 grass (C3) and C4 grass (C4).

[1]Latham and Schlieter (1989), [2]Li et al. (2012b), [3]Arora and Boer (2005), [4]Thonicke et al. (2010), [5]Pechony and Shindell (2009), [6]own work

Every fire counted spreads in an elliptical shape where the longest axis is in the downwind direction. The length-to-breadth ratio L_B is estimated by

$$L_B = 1 + 10 \cdot (1 - e^{-0.06w}) \tag{11}$$

where w is the wind speed in ms^{-1} (Arora and Boer, 2005).

The head-to-back ratio HB is given by

$$H_B = \frac{L_B + (L_B^2 - 1)^{1/2}}{L_B - (L_B^2 - 1)^{1/2}} \tag{12}$$

https://doi.org/10.5194/egusphere-2022-961
Preprint. Discussion started: 1 November 2022

(Li et al., 2012b).

Fire spread rate in the downwind direction u_w (ms^{-1}) is

$$u_w = 2u_{max,i} \cdot f_{RH} \cdot f_{root} \cdot g(w) \tag{13}$$

where $u_{max,i}$ is the maximum fire spread rate in natural vegetation regions for vegetation type i and f_{root} and $g(w)$ are functions of soil moisture and wind speed respectively and vary between 0 and 1 (Li et al., 2012b). f_{root} is a surrogate for vegetation moisture content (Arora and Boer, 2005). The 2x factor comes from the corrigendum of Li et al., 2012a. In Li et al., 2012b, f_{root} is dependent on the water content of the different soil layers associated with different vegetation types. Since the land surface scheme of the UVic model is single layered (Meissner et al., 2003), f_{root} will be constant among plant functional types.

f_{root} is given by

$$f_{root} = 1 - tanh\left(\frac{1.75\beta_{root}}{\beta_e}\right)^2 \tag{14}$$

where β_{root} is the availability of water in the soil and β_e is an extinction wetness constant above which the probability of fire is negligible (Arora and Boer, 2005).

$beta_{root}$ is given by

$$\beta_{root} = max\left[0, min\left(1, \frac{\theta - \theta_w}{\theta_c - \theta_w}\right)\right] \tag{15}$$

where θ_w is the wilting soil moisture content (the volumetric soil moisture concentration below which stomata close) and θ_c is the critical soil moisture content (the volumetric soil moisture concentration above which stomata are not sensitive to soil water) (Arora and Boer, 2005).

$g(w)$ is given by

$$g(w) = \frac{2L_B}{1 + \frac{1}{H_B}} g(0) \tag{16}$$

(Li et al., 2012b), where $g(0)$ is a constant.

The fire spread rate perpendicular to the wind u_p is

$$u_p = u_{max} \cdot g(0) \cdot f_{root} \cdot f_{RH} \tag{17}$$

(Li et al., 2012b).

https://doi.org/10.5194/egusphere-2022-961
Preprint. Discussion started: 1 November 2022

The average burned area B_a (km^2) of a single fire is then defined according to the formula for the area of an ellipse, namely,

$$B_a = \frac{\Pi \cdot u_w^2 \cdot t^2}{4L_B} \cdot (1 + \frac{1}{H_B})^2 \cdot \Omega \cdot 10^{-6} \tag{18}$$

(Li et al., 2012b), where t is the average fire duration in seconds, Ω is an adjustment factor and 10^{-6} converts m^2 to km^2.

The burned area B_A (km^2) in the grid cell is then the product of the number of fires with the average burned area per fire,

$$B_A = N_f \cdot B_a \tag{19}$$

where N_f is the number of fires.

2.3.3 Fire impacts

Once the burned fraction has been calculated, it is applied to the vegetation fraction for each PFT taking into account that woody PFTs will not burn completely because of islands of vegetation that remain unburned (Landry et al., 2015, Supplementary material). This amounts to a 5% difference between modelled gross and net burned area. Fire-caused emissions, consisting of CO_2, non-CO_2, aerosols and pyrogenic carbon emissions, are then calculated and allocated to the other modules (Landry et al., 2015).

2.4 Improvements to the UVic ESCM climatology

To improve the simulated climatology of the UVic ESCM, we created a proxy for the simulated relative humidity based on simulated precipitation and we added observationally-derived variability to the two main climate variables used by the fire model, relative humidity and soil moisture. We also performed simulations using prescribing observational relative humidity as input to the fire model, to assess the degree of adequacy of our precipitation proxy.

2.4.1 Relative humidity

Relative humidity simulated in the UVic ESCM is almost perfectly homogeneous spatially and temporally because of the use of a constant relative humidity threshold of 0.85 to generate precipitation in the model (Fig. 3**a**). To improve its spatial variability, we used the more variable simulated precipitation to derive a relative humidity field as follows:

$$RH_{sim} = \begin{cases} 0 & \text{if } PR_{sim} \leq PR_{min} \\ \frac{PR_{sim} - PR_{min}}{PR_{max} - PR_{min}} & \text{if } PR_{min} < PR_{sim} < PR_{max} \\ 1 & \text{if } PR_{sim} \geq PR_{max} \end{cases} \tag{20}$$

where RH_{sim} is the relative humidity field used in the fire model, PR_{sim} is the simulated precipitation, PR_{min} and PR_{max} are arbitrary precipitation value thresholds determining the null and saturated relative humidity. These two values

https://doi.org/10.5194/egusphere-2022-961
Preprint. Discussion started: 1 November 2022

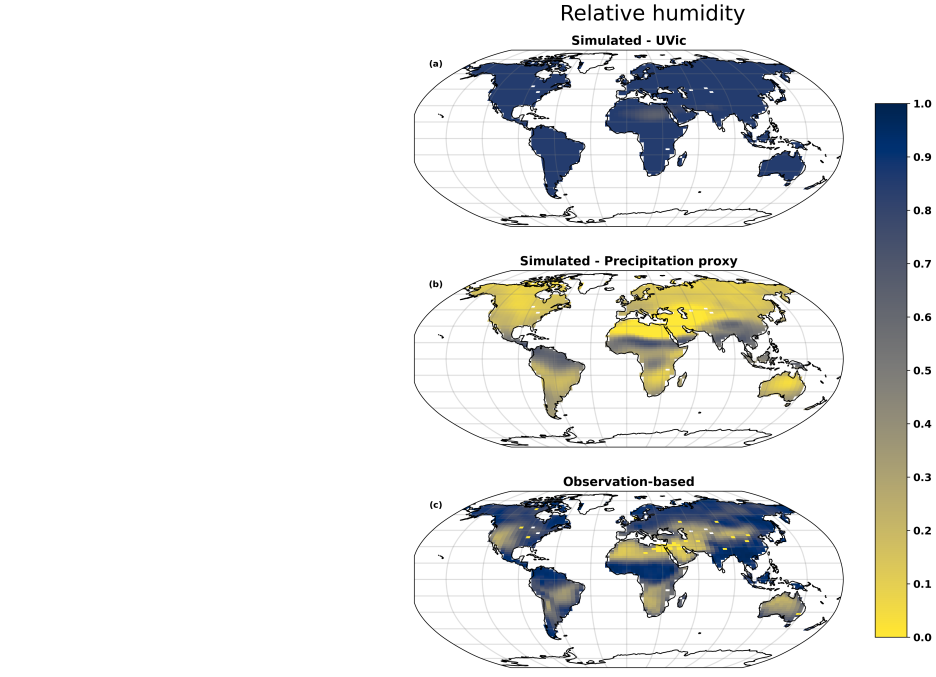

Figure 3. Relative humidity for the month of August (a) simulated by the UVic ESCM (constant at 0.85 over most land surface and every month), (b) estimated using the simulated precipitation as a proxy and (c) based on observation. For all months, see Fig.4.

(Table 1) correspond to annual extremes of a desert climate (PR_{min}) and a semi-arid climate (PR_{max}). They were chosen to optimize the seasonal and spatial variability of the relative humidity field generated by the simulated climatology (Fig. 4). The precipitation-proxied relative humidity (Fig. 3**b**) greatly improves on the default UVic simulated relative humidity (Fig. 3**a**) in terms of spatial pattern and variability and in terms of seasonal variability (Fig. 4). The discrepancy with observation-based relative humidity (Fig. 3**c**, Fig. 4) is however still important. We therefore also included simulations using monthly observational relative humidity, as input to the fire model.

2.4.2 Natural variability

The monthly simulated soil moisture (SM_{sim}) and relative humidity (RH_{sim}) display significantly less variability than observational variability (Fig. 4 & Fig. 5, respectively). We included simulation runs where the standard deviation of observed precipitation and soil moisture products were added to the simulated values (Fig. 4 & Fig. 5, respectively). A visual analysis of histograms showed that both monthly-averaged precipitation and soil moisture were generally normally distributed across the observation periods, validating the use of the observational standard deviation. Every fire step, when variability was added, the precipitation and soil moisture used in the fire model in a grid cell were given by

$$PR_{simsd} = PR_{sim} + SD_{PR} \cdot rndnum \; ; \; PR_{simsd} \geq 0 \tag{21}$$

https://doi.org/10.5194/egusphere-2022-961
Preprint. Discussion started: 1 November 2022

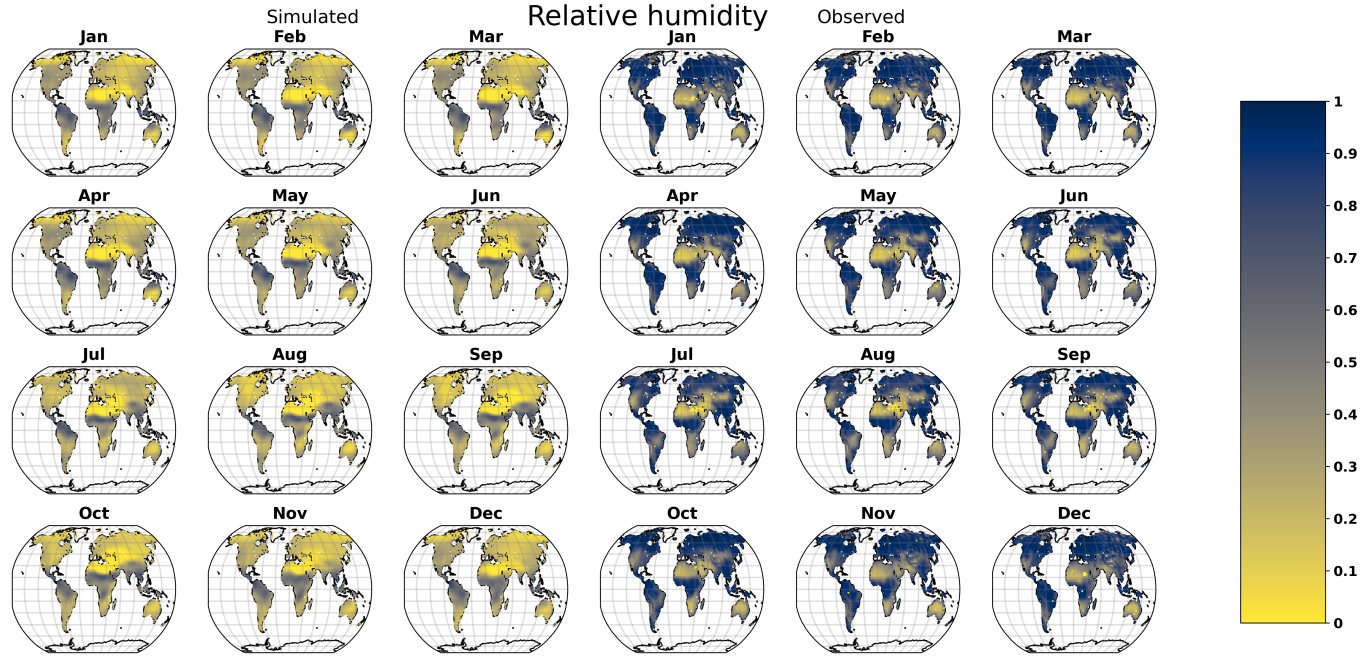

Figure 4. Relative humidity, precipitation-proxied and observed. Precipitation-proxied relative humidity is based on simulated precipitation.

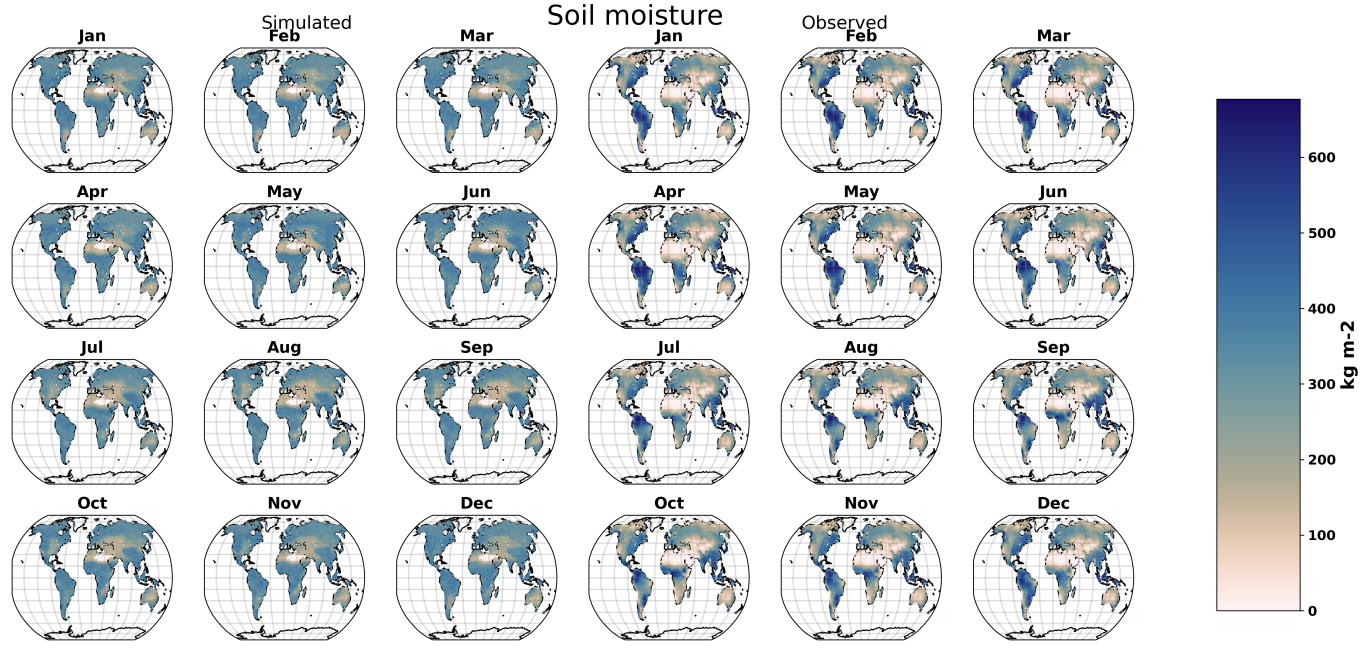

Figure 5. Soil moisture, simulated and observed. Simulated soil moisture has added observational variability.

https://doi.org/10.5194/egusphere-2022-961
Preprint. Discussion started: 1 November 2022

Variable	units	averaging period	source
	Prescribed		
Lightning rate	flashes $\mathrm{km}^{-2}\mathrm{month}^{-1}$	1995-2013	Cecil et al. (2014)
Population density	people km^{-2}	2000	Jones and O'Neill (2016)
Precipitation variability	$\mathrm{mmmonth}^{-1}$	1901-2013	Schneider et al. (2014)
Soil moisture variability	kgm^{-2}	1948-2016	Fan and Van Den Dool (2004)
Crop and pasture lands	fraction of gridcell	2005	UVic ESCM default
	Model validation		
Fire counts	no of fires $\mathrm{km}^{-2}\mathrm{month}^{-1}$	2001-2006	Giglio et al. (2006)
Burned fraction	fraction of gridcell month^{-1}	2001-2012	Giglio et al. (2013) (GFED4)
Relative humidity	unitless	1948-2014	Kalnay et al. (1996)
Soil moisture	kgm^{-2}	1948-2016	Fan and Van Den Dool (2004)
Aboveground biomass density	kgCm^{-2}	1960-2000 period	Olson et al. (2001)

Table 2. Description of datasets used for forcing and validation.

$$SM_{simsd} = SM_{sim} + SD_{SM} \cdot rndnum \; ; \; SM_{simsd} \geq 0 \tag{22}$$

where PR_{simsd} and SM_{simsd} are the simulated precipitation and soil moisture with added observational variability, sd their respective monthly standard deviation and $rndnum$ is a random normal number, identical for precipitation and soil moisture pairs and taken from a standard normal distribution (mean = 0, standard deviation = 1).

We also added observational variability to the prescribed relative humidity simulations the same way as for precipitation (eq.(21))

$$RH_{obssd} = RH_{obs} + SD_{RH} \cdot rndnum \; ; \; RH_{obssd} \geq 0 \tag{23}$$

where RH_{obssd} is the relative humidity with added variability prescribed to the fire model, RH_{obs} is the monthly observational relative humidity and SD_{RH} is the monthly relative humidity observational standard deviation.

2.5 Parameter optimization

In order to accomodate the monthly timestep and coarser resolution of the UVic ESCM relative to the original parameterization (Li et al., 2012b), we adjusted the fire model parameters from the literature (Table 1) to optimize, step by step, the simulated ignitions, then fire counts and finally the burned area. We performed this optimization process for a model using the simulated precipitation relative humidity proxy ($rhsim$) and a model using prescribed relative humidity ($rhobs$). The $base$ model (default

https://doi.org/10.5194/egusphere-2022-961
Preprint. Discussion started: 1 November 2022

parameterization) and the parameterized models are described in Table 1. Based on this preliminary optimization, we then tested the effect of adding variability to relative humidity and soil moisture, as well the effect of multiplying the final burned area by a constant factor Ω, leading to a multi-model comparison.

2.6 Simulation settings

Each simulation ran for up to 2000 years with constant forcings, until the models had reached equilibrium in terms of burned area versus vegetation regrowth. We used pre-industrial atmospheric CO_2 concentration and other climate forcings, but contemporary agricultural fractions (year 2005) and population density (beginning of the 21st century) (Table 2). As a benchmark to evaluate the fire parameterizations, we used the burned fraction product from the version 4 of the Global Fire Emissions Database (GFED4) (Giglio et al., 2013), which spans the 2001-2010 period. The global burned area of GFED4 amounts to $350\mathrm{Mha/yr}$, $4\mathrm{Mha/yr}$ of which corresponds to deforestation fires (based on Van der Werf et al., 2010). GFED4 does not detect small fires that have been estimated to affect $120\mathrm{Mha/yr}$, mostly (80%) from croplands, savannahs and grasslands (Randerson et al., 2012). To compare the different model versions, we used the monthly burned fraction and above-ground vegetation carbon and the yearly global totals for burned area and aboveground vegetation carbon for the last 20 years of each simulation.

3 Results

The fully coupled model, using simulated precipitation as a proxy for relative humidity ($rhsimSmRh$ in Fig.8, hereafter $rhsim$), simulates burned fraction with a moderate global agreement with GFED4 (Fig. 6a) (r=0.39) and underestimates global burned area by about 50%. The model generally overestimates the spatial extent and underestimates the spatial variability of burned fraction (Fig. 6b). The equatorial region of *Northern Hemisphere Africa* and *Southern Hemisphere Africa*, *Northern South America* and *Equatorial Asia* (for map of regions, see Fig.9**c**) are particularly affected by this bias; there the model strongly overestimates burned fraction. This over-burning pattern is a direct consequence of the precipitation-proxied relative humidity input, which, while it definitely improves on the default relative humidity simulation, does not quite reproduce the permanently water saturated atmosphere of those tropical rainforest regions (Fig.4). The model using observation-based relative humidity ($rhobsX2SmRh$ in Fig.8, hereafter $rhobs$) corrects this bias and confirms the predominant role of relative humidity in these regions (Fig.6c).

The simulated vegetation reflects the model simulated fire patterns, with a complete burn down of the vegetation in the equatorial African rainforest region and the significant reduction of vegetation density in Northern South America (Fig. 7b). In other regions, the $rhsim$ model partially reproduces the higher burned fractions in *North* and *South Africa* savannas and in *Southern South America*, and more correctly the high burned fraction in *northern Australia*, but not always quite to the same order of magnitude as observations (Fig. 6, note the log-transformed axis). The strong discrepancies in North and South Africa can be explained, again, partly by the lack of variability of the model's precipitation-proxied relative humidity across these regions, which limited the potential to increase the effect of low relative humidity (RH_{low}) and low soil moisture (θ_e) on fire

https://doi.org/10.5194/egusphere-2022-961
Preprint. Discussion started: 1 November 2022

activity during the optimization phase (see Table 1 for differences in parameterization between the $rhsim$ and $rhobs$ models). In *Boreal North America* and *Boreal Asia*, burned area is underestimated following an overestimate of soil moisture in the warm season (Fig. 5).

Other notable simulated burned area biases can be attributed to biases in the simulated vegetation of the UVic ESCM. The most important of these vegetation-induced biases is in *Temperate North America*, where both models overestimate fire activity, $rhsim$ more in terms of spatial extent and $rhobs$ more in terms of intensity. There are two reasons for this. First, vegetation and precipitation are overestimated by the UVic ESCM-TRIFFID in this region (see Fig. 5 & 7 in Mengis et al., 2020, see also Fig.1**b** vs. **c** in this paper); this leads to higher fuel loads in a relatively still dry (in relation to the parameterization of the models) region, the perfect conditions for biomass burning. Moreover, in the $rhobs$ model, the prescribed relative humidity informing the fire model is even drier (Fig.4), while the TRIFFID vegetation model receives an overestimated simulated precipitation input, creating an environment that is very arid for fire yet highly productive for vegetation, a virtual haven for high burned fractions to occur (Fig. 6c). The second reason is that a lot of the vegetated area in *Temperate North America* is flammable cropland, which is treated as natural vegetation by the current fire parameterization, leading to an overestimation of burned area (see Li et al. (2013) for a parameterization of agriculture fires). In *western Central Asia* high burned fractions occur due to agriculture, a large part of which is not captured by our model because the UVic ESCM simulates no or very little vegetation in this area.

In summary, the main discrepancies between the simulated and observed burned area are due to seasonal and regional biases and low variability of the simulated climate and vegetation in the UVic ESCM.

3.1 Effect of improvements

The results presented in Fig.6-7 were made possible by several modifications to the simulated climatology and the fire model parameters. The modification of the simulated relative humidity by using the more variable simulated precipitation field as a proxy greatly improved the variability of the simulated burned fraction (Fig.8, $rhsimBASE$ vs. $rhUVIC$). The spatial correlation of fire activity was significantly increased by optimizing the parameterization of the fire model, though at the cost of losing a lot of variability (Fig.8, $rhsimNOSD$ vs. $rhsimBASE$).

Our results from the previous section indicate that using monthly simulated climatology rather than the daily to subdaily timestep the current fire model was designed for (Li et al., 2012b), still allows to capture many broad patterns of fire activity. This requires emulating temporal variability with the use of natural variability, which significantly improves the simulated burned fraction, both in terms of spatial correlation and spatial variability relative to observations (Fig. 8, $rhsimSmRh$ vs. $rhsimNOSD$). Natural variability, however, is only a partial substitute for fine-scale temporal variability, bringing the normalized standard deviation from about 0.1 to 0.25.

Soil moisture natural variability alone brought significant improvements to the model (Fig.8, $rhsimSm$ vs $rhsimNOSD$) while relative humidity variability decreased (Fig.8, $rhsimRh$ vs $rhsimNOSD$) or did not improve (Fig.8, $rhsimRhX2$ vs $rhsimNOSD$) the performance of the model at simulating burned area. In conjunction with soil moisture variability, however,

https://doi.org/10.5194/egusphere-2022-961
Preprint. Discussion started: 1 November 2022

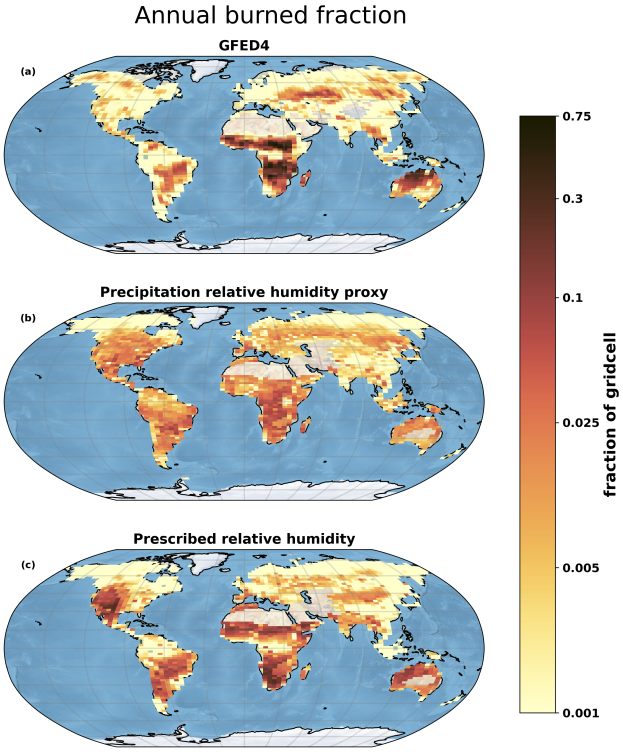

Figure 6. Final models with (a) fully simulated climatology (relative humidity is proxied with simulated precipitation) and (b) prescribed relative humidity. (c) Benchmark using prescribed observational dataset for burned fraction.

relative humidity variability further improved the model (Fig.8, $rhsimSmRh$ vs $rhsimNOSD$). This highlights fire activity as dependent on the interaction of both these climate drivers.

In the selection process for the best models, both for the fully simulated climatology ($rhsim$) and the prescribed relative humidity ($rhobs$) ensembles, one of the main tradeoffs that guided our choice was the ability of the model to preserve the simulated vegetation relative to the simulation with prescribed observational burned fraction ($GFED4$). The final $rhsim$ model ($rhsimSmRh$ in Fig.8) , which had its climatology inputs complemented by both relative humidity and soil moisture natural variability, displays a burned fraction pattern and variability that mostly preserves the simulated vegetation. This model was retained instead of the $rhsimX2SmRh$, which represents more spatial variability for burned fraction but not in the correct locations, as can be attested from the large decrease it brings to the agreement of simulated vegetation with observations (Fig. 8). The final $rhobs$ ($rhobsX2SmRh$ in Fig.8) model also benefited from the addition of both relative humidity and soil moisture natural variability, as well as having its output burned fraction multiplied by two. We understand the relevance of $\Omega = 2$ factor as an indication that the spatial pattern of burned area is in better agreement with observational data when relative humidity is prescribed. Since the addition of natural variability for climate inputs only partially substitutes for their lack of fine-scale temporal variability, Ω further contributes as a substitute. Given the higher spatial agreement, this improves the

https://doi.org/10.5194/egusphere-2022-961
Preprint. Discussion started: 1 November 2022

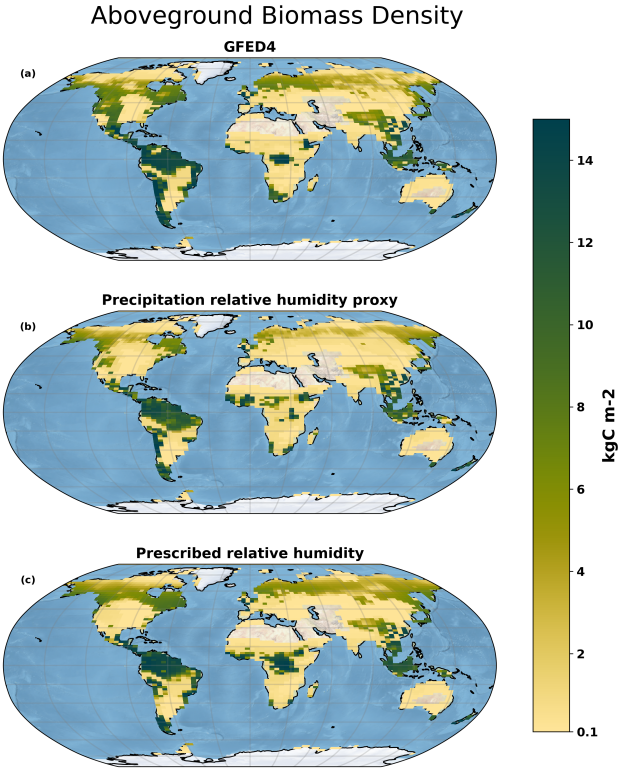

Figure 7. Final models with (a) fully simulated climatology (relative humidity is proxied with simulated precipitation) and (b) prescribed relative humidity. (c) Benchmark using prescribed observational dataset for burned fraction.

simulated global burned area (Fig.9**a**) without increasing the spatial bias of the simulated vegetation (Fig.8). $rhobs$, however, does not reach a spatial correlation of burned area with observations higher than $rhsim$ (Table 3). This can be attributed to the discrepancy mentioned earlier in the $rhobs$ model set; relative humidity driving the simulated vegetation is not the same as the one which drives fire activity, the former is simulated and biased while the second is prescribed, leading to potential bias in the simulated fire activity.

4 Discussion

The goal of this study was to assess the feasibility of the fully coupled and spatially explicit simulation of annual burned area in an earth system model of intermediate complexity. Our results demonstrate that it is possible to partially substitute for the limited temporal variability of the simulated climatology by complementing relative humidity and soil moisture with their natural variability. This method does not however address the spatial variability or the spatial bias of the simulated climatology. In particular, relative humidity as simulated by using UVic-simulated precipitation as a proxy lacks spatial variability in the African tropics, leading to a strong overestimation of fire activity in the central African rainforests. This demonstrates that

https://doi.org/10.5194/egusphere-2022-961
Preprint. Discussion started: 1 November 2022

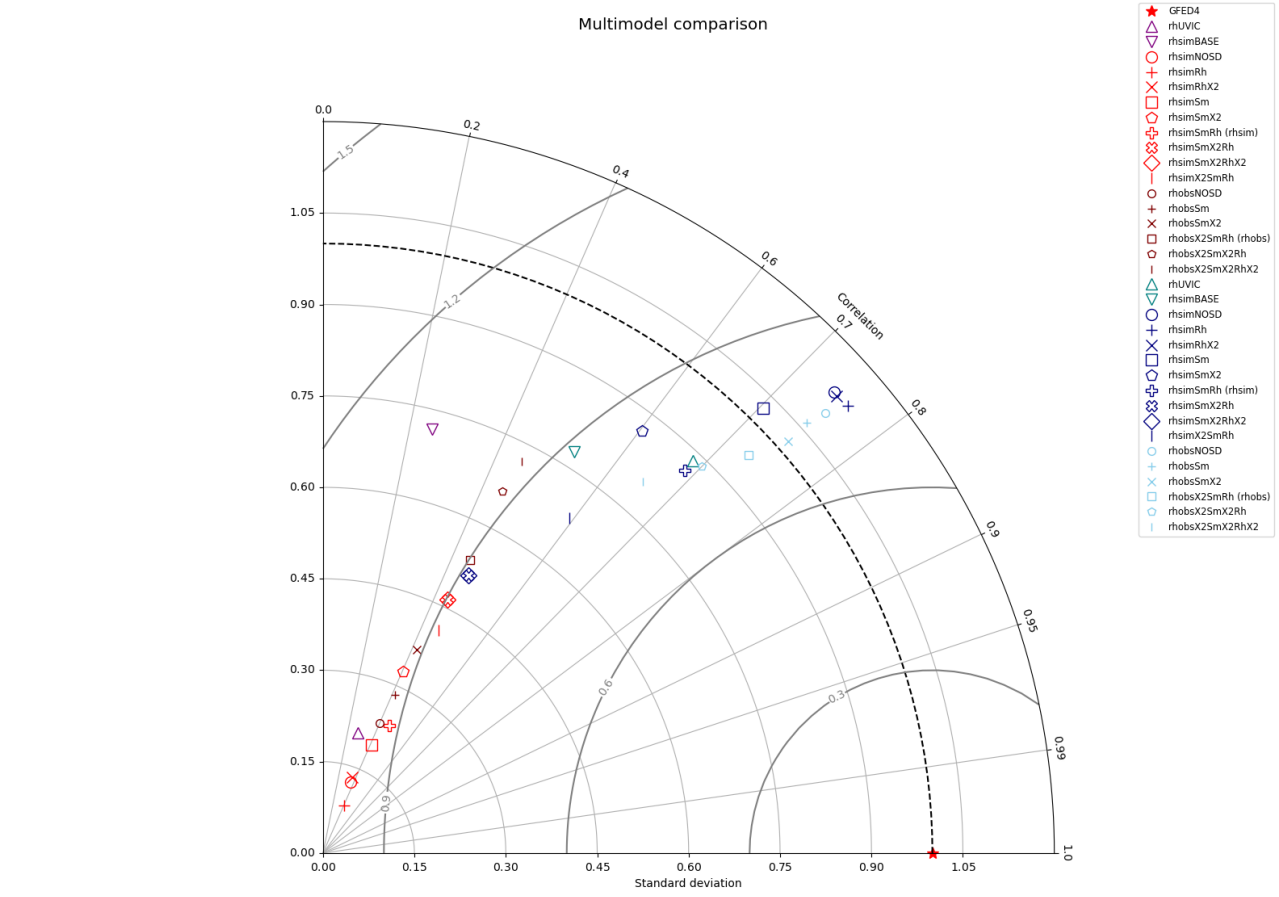

Figure 8. Taylor Diagram (Taylor, 2001) of simulated Burned Fraction (purple/red/brown), correlation uses log-transformed values) and Aboveground Carbon Biomass Density (green/blue/light blue) for simulated and prescribed relative humidity model sets. Data is normalized to standard deviation. **GFED4**: benchmark burned fraction observation-based dataset; **rhUVIC**: default parameterization and constant relative humidity function FUN_{RH}=0.5 as per the default relative humidity simulated by the UVic ESCM; **BASE**: default parameterization (all other models except rhUVIC have been parameterized to optimize burned fraction); **rhsim[...]**: precipitation relative humidity proxy models; **rhobs[...]**: prescribed relative humidity models; **NOSD**: no natural variability; **Rh**: relative humidity natural variability added (monthly standard deviation); **Sm**: soil moisture natural variability added (monthly standard deviation); **X2**: preceding term multiplied by 2 (X2 after rhsim or rhobs means that final burned area has been multiplied by 2).

relative humidity plays a key role in maintaining tropical rainforests fire-free. When relative humidity is prescribed, clear improvements occur in particular with regards to the contrasting fire activity between the adjacent African savannas (high
350 burned area) and rainforest (fire-free) regions (see Fig.6). Global burned area, which is largely controlled by African vegetation

https://doi.org/10.5194/egusphere-2022-961
Preprint. Discussion started: 1 November 2022

Model	global burned area ($MHayr^{-1}$)	r (log)	GVC (PgC)	r
rhsim	167	0.39 (0.46)	322	0.69
rhobs	275	0.24 (0.45)	385	0.73
obs	330	1 (1)	404	1

Table 3. Main results for the fully coupled model $rhsim$, using simulated precipitation as a proxy for relative humidity, the model $rhobs$ using prescribed relative humidity, and the model using prescribed burned fraction observations based on GFED4. GBA: Global Burned Area; GVC: Global Vegetation Carbon (aboveground); r: spatial correlation with observations; (log) designates spatial correlation of the log-transformed burned area.

fires (66%; 1997-2004; van der Werf et al., 2006), is then much more in line with observations (Fig.9), generally without sacrificing spatial agreement elsewhere (see $rhobsX2SmRh$ vs. $rhsimSmRh$ in Fig.8).

4.1 Comparison with other studies

Albeit one exception (Wu et al., 2021), we are not aware of any other EMICs coupled to a fire model. Before making comparisons, we can approximate the potential spatial correlation of burned area with observations that can be achieved by our model based on the simulated vegetation, on which fire activity largely depends. The vegetation carbon density simulated by the vegetation module TRIFFID when burned area is prescribed, is in moderate agreement with observations (r=0.30, Fig.1a). The present study yields a global spatial correlation of burned area close to this value (r=0.39). The original fire parameterization of this study, using prescribed observation-based daily to sub-daily climate inputs that informed the simulated vegetation at equilibrium, yielded a higher global spatial correlation (r=0.60; Li et al., 2012b). Moreover, Li et al., 2012b are able to reproduce the main features of global burned area, in particular the high fraction in tropical savannas and very low fraction in tropical rainforests (see Fig.8 of their paper). An earlier parameterization using an hybrid statistical-process approach and prescribing monthly climate inputs yielded similar results to our study; a moderate global spatial correlation for burned fraction and mixed per-region agreement (Glob-FIRM in Thonicke et al., 2010; r=0.39). The current model obtains a global burned area closer to observations at 167 $\mathrm{Mha/yr}$ or 50% underestimation of GFED4, instead of 54 $\mathrm{Mha/yr}$ for Glob-FIRM, while Li et al., 2012b underestimate GFED3 (Giglio et al., 2010) by <15%.

4.2 Limitations

Generally, integrating modules by coupling them increases the complexity of the model and the uncertainty of its outputs, and when temporal and spatial scales differ, this can affect the parameterization and require a more difficult calibration (Voinov and Shugart, 2013). In the present study, we coupled a daily timestep fire model to a monthly timestep climate-vegetation model.

https://doi.org/10.5194/egusphere-2022-961
Preprint. Discussion started: 1 November 2022

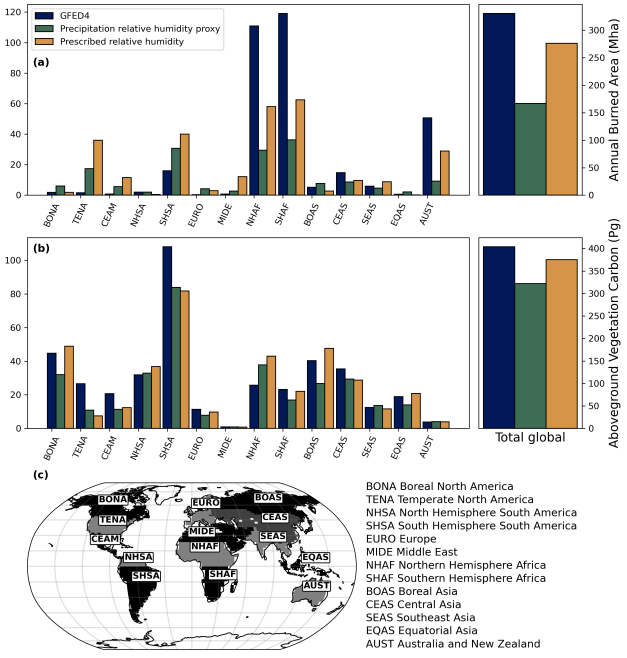

Figure 9. (a) Simulated annual burned area; (b) Simulated aboveground vegetation carbon; (c) Map of the 14 regions used in this study at the model resolution (100x100), after Giglio et al. (2006), van der Werf et al. (2006) and Van der Werf et al. (2010).

Our final fully coupled model $rhsim$ is the best version of the model given the limitations of model-simulated climate and vegetation variables.

An important limitation to note is the ability of the UVic ESCM to simulate present day vegetation carbon density patterns. It appears that the UVic ESCM was calibrated to simulate vegetation potential in the absence of fire, given that its simulation of vegetation in the absence of fire correlates slightly better with observed vegetation (r=0.33, Fig.1**b**) than its simulation of vegetation with prescribed observed fire (r=0.30, Fig.1**a**)

To demonstrate the importance of the spatial pattern of relative humidity in determining fire activity, especially in the carbon rich tropical rainforests, we used prescribed relative humidity. Other than this direct influence of the simulated climate, biases in terms of spatial pattern and intensity of simulated burned area can be attributed to the indirect influence of climate on simulated vegetation and the limited ability of the vegetation model to represent global vegetation patterns.

One area of improvement that could be implemented in future model versions is to differentiate between fires in agricultural regions and those in natural vegetation areas. Agriculture biomass burning, deforestation and peat fires, account for less than 10% of global annual burned area but nearly 40% of emissions (Li et al., 2013). Deforestation in particular is common in carbon-dense tropical regions and thus contributes disproportionately to fire-caused emissions.

Another notable limitation to our study that could be improved upon is fire duration. Although vegetation fires last on average one day (Venevsky et al., 2002), savanna fires in particular are very long-lived (Andela et al., 2019). A fire duration

https://doi.org/10.5194/egusphere-2022-961
Preprint. Discussion started: 1 November 2022

parameterization (e.g. Pfeiffer et al., 2013; Le Page et al., 2015) could correct for the underestimation bias of burned fraction in these regions.

5 Conclusions

The main objective of this study was to assess the feasibility of coupling a global fire model in an EMIC, with the goal of improving its century-scale temperature projections by the inclusion of fire-caused emissions in its carbon cycle. We used a fire model parameterized to represent fire activity variability at the decadal to centennial scales, due to its focus on precipitation-related inputs (Pechony and Shindell, 2010), namely relative humidity and soil-moisture (Li et al., 2012b; Fig.2). Our study is unique in that we used the simplified atmospheric module of the UVic ESCM, which simulates atmospheric processes with monthly variability, to drive the fire-DGVM model, while other fire models prescribed daily (Thonicke et al., 2010) or sub-daily (Li et al., 2012b) climatology data to drive their fire-DGVM. Our results suggest that temporal variability is crucial to inform the fire model, and that adding natural variability to data at longer timesteps can serve as a substitute for the variability intrinsic to shorter timesteps. However, this does not address issues that arise from poor accuracy of regional patterns. The UVic ESCM as it stands has many biases in terms of its simulated climate that have direct effects on simulated fire and indirect effects through vegetation.

Our success in improving simulated fire patterns using prescribed relative humidity points to one promising solution: using pattern scaling to emulate climatology based on the linear relationship of climate variables with the EMIC-simulated temperature. Wu et al. (2021) use IMOGEN, an EMIC that emulates monthly climatology using pattern scaling based on CMIP5 climatology data, to which they couple a fire-DGVM model. This solution not only improves the simulated climatology inputs, but also indirectly the simulated vegetation. Pattern scaling would greatly improve the current model, however it is no panacea; linear scaling only explains (in IMOGEN) 15% of precipitation variability as simulated by CMIP5, and relative humidity has the highest uncertainty of all variables in terms of the magnitude of change (Zelazowski et al., 2018). It would also be possible to simply pattern scale relative humidity, but the issues with vegetation biases propagating in the simulated fire activity would partially remain due to biases in other climate variables related to relative humidity, such as precipitation. Nevertheless, pattern-scaling as described by Wu et al. (2021) is a promising way to achieve a sensible representation of the global fire activity patterns in EMICs.

Code and data availability. The code modifications and additions to the UVic ESCM 2.9 model, the input, calibration and validation datasets, the simulation output files as well as the code used for analysis and to produce the figures are available at https://www.doi.org/10.20383/103.0647. The references for the data used as input and for calibration and validation are detailed in Table 2. The code for the UVic ESCM 2.9 model can be found at http://terra.seos.uvic.ca/model/.

https://doi.org/10.5194/egusphere-2022-961
Preprint. Discussion started: 1 November 2022

Author contributions. ÉG collected the data, programmed the model, performed the simulations and wrote the manuscript; both authors contributed to the design of the model and discussed the results; HDM contributed to the supervision of the work and reviewed the final manuscript.

Competing interests. The authors declare no competing interests.

Acknowledgements. The authors wish to thank Jean-Sébastien Landry for his suggestions in designing the implementation of the fire model in the UVIC ESCM, Michael Eby for his help with debugging the model, Corey Lesk for his comments on the structure of an earlier draft of the manuscript and Yannick Copin for his python code to produce the Taylor Diagram visuals. This research was funded by a Concordia University Graduate Fellowship.

https://doi.org/10.5194/egusphere-2022-961
Preprint. Discussion started: 1 November 2022

References

Andela, N., Morton, D. C., Giglio, L., Paugam, R., Chen, Y., Hantson, S., Van Der Werf, G. R., and Randerson, J. T.: The Global Fire Atlas of individual fire size, duration, speed and direction, Earth System Science Data, 11, 529–552, 2019.

Andreae, M. O. and Merlet, P.: Emission of trace gases and aerosols from biomass burning, Global biogeochemical cycles, 15, 955–966, 2001.

Arora, V. K. and Boer, G. J.: Fire as an interactive component of dynamic vegetation models, Journal of Geophysical Research: Biogeosciences, 110, 2005.

Bistinas, I., Harrison, S., Prentice, I., and Pereira, J.: Causal relationships versus emergent patterns in the global controls of fire frequency, Biogeosciences, 11, 5087–5101, 2014.

Bowman, D. M., Balch, J. K., Artaxo, P., Bond, W. J., Carlson, J. M., Cochrane, M. A., D'Antonio, C. M., DeFries, R. S., Doyle, J. C., Harrison, S. P., et al.: Fire in the Earth system, science, 324, 481–484, 2009.

Cecil, D. J., Buechler, D. E., and Blakeslee, R. J.: Gridded lightning climatology from TRMM-LIS and OTD: Dataset description, Atmospheric Research, 135, 404–414, 2014.

Ciais, P., Sabine, C., Bala, G., and Peters, W.: Carbon and Other Biogeochemical Cycles, pp. 465–570, Cambridge University Press, https://doi.org/10.1017/CBO9781107415324.015, complete rapport op http://www.climatechange2013.org/report/, 2013.

Claussen, M., Mysak, L., Weaver, A., Crucifix, M., Fichefet, T., Loutre, M.-F., Weber, S., Alcamo, J., Alexeev, V., Berger, A., et al.: Earth system models of intermediate complexity: closing the gap in the spectrum of climate system models, Climate dynamics, 18, 579–586, 2002.

Cox, P. M.: Description of the" TRIFFID" dynamic global vegetation model, 2001.

Ding, Z., Peng, J., Qiu, S., and Zhao, Y.: Nearly half of global vegetated area experienced inconsistent vegetation growth in terms of greenness, cover, and productivity, Earth's Future, 8, e2020EF001 618, 2020.

Eby, M., Zickfeld, K., Montenegro, A., Archer, D., Meissner, K., and Weaver, A.: Lifetime of anthropogenic climate change: Millennial time scales of potential CO 2 and surface temperature perturbations, Journal of climate, 22, 2501–2511, 2009.

Fan, Y. and Van Den Dool, H.: Climate Prediction Center global monthly soil moisture data set at 0.5 resolution for 1948 to present, Journal of Geophysical Research: Atmospheres, 109, 2004.

Giglio, L., Csiszar, I., and Justice, C. O.: Global distribution and seasonality of active fires as observed with the Terra and Aqua Moderate Resolution Imaging Spectroradiometer (MODIS) sensors, Journal of geophysical research: Biogeosciences, 111, 2006.

Giglio, L., Randerson, J., Van der Werf, G., Kasibhatla, P., Collatz, G., Morton, D., and DeFries, R.: Assessing variability and long-term trends in burned area by merging multiple satellite fire products, Biogeosciences, 7, 1171–1186, 2010.

Giglio, L., Randerson, J. T., and Van Der Werf, G. R.: Analysis of daily, monthly, and annual burned area using the fourth-generation global fire emissions database (GFED4), Journal of Geophysical Research: Biogeosciences, 118, 317–328, 2013.

Hantson, S., Arneth, A., Harrison, S. P., Kelley, D. I., Prentice, I. C., Rabin, S. S., Archibald, S., Mouillot, F., Arnold, S. R., Artaxo, P., et al.: The status and challenge of global fire modelling, Biogeosciences, 13, 3359–3375, 2016.

Hantson, S., Kelley, D. I., Arneth, A., Harrison, S. P., Archibald, S., Bachelet, D., Forrest, M., Hickler, T., Lasslop, G., Li, F., et al.: Quantitative assessment of fire and vegetation properties in simulations with fire-enabled vegetation models from the Fire Model Intercomparison Project, Geoscientific Model Development, 13, 3299–3318, 2020.

https://doi.org/10.5194/egusphere-2022-961
Preprint. Discussion started: 1 November 2022

Jolly, W. M., Cochrane, M. A., Freeborn, P. H., Holden, Z. A., Brown, T. J., Williamson, G. J., and Bowman, D. M.: Climate-induced variations in global wildfire danger from 1979 to 2013, Nature communications, 6, 1–11, 2015.

Jones, B. and O'Neill, B. C.: Spatially explicit global population scenarios consistent with the Shared Socioeconomic Pathways, Environmental Research Letters, 11, 084 003, 2016.

Jones, M. W., Santín, C., van der Werf, G. R., and Doerr, S. H.: Global fire emissions buffered by the production of pyrogenic carbon, Nature Geoscience, 12, 742–747, 2019.

Kalnay, E., Kanamitsu, M., Kistler, R., Collins, W., Deaven, D., Gandin, L., Iredell, M., Saha, S., White, G., Woollen, J., et al.: The NCEP/NCAR 40-year reanalysis project, Bulletin of the American meteorological Society, 77, 437–472, 1996.

Kasoar, M., Hamilton, D., Dalmonech, D., Hantson, S., Lasslop, G., Voulgarakis, A., and Wells, C.: Improved estimates of future fire emissions under CMIP6 scenarios and implications for aerosol radiative forcing, in: EGU General Assembly Conference Abstracts, pp. EGU21–13 822, 2021.

Kelley, D. I., Bistinas, I., Whitley, R., Burton, C., Marthews, T. R., and Dong, N.: How contemporary bioclimatic and human controls change global fire regimes, Nature Climate Change, 9, 690–696, 2019.

Kloster, S., Mahowald, N. M., Randerson, J. T., Thornton, P. E., Hoffman, F. M., Levis, S., Lawrence, P. J., Feddema, J. J., Oleson, K. W., and Lawrence, D. M.: Fire dynamics during the 20th century simulated by the Community Land Model, Biogeosciences, 7, 1877–1902, 2010.

Kloster, S., Mahowald, N., Randerson, J., and Lawrence, P.: The impacts of climate, land use, and demography on fires during the 21st century simulated by CLM-CN, Biogeosciences, 9, 509–525, 2012.

Knorr, W., Jiang, L., and Arneth, A.: Climate, CO 2, and demographic impacts on global wildfire emissions., Biogeosciences Discussions, 12, 2015.

Landry, J.-S. and Matthews, H. D.: Non-deforestation fire vs. fossil fuel combustion: the source of CO 2 emissions affects the global carbon cycle and climate responses, Biogeosciences, 13, 2137–2149, 2016.

Landry, J.-S. and Matthews, H. D.: The global pyrogenic carbon cycle and its impact on the level of atmospheric CO 2 over past and future centuries, Global change biology, 23, 3205–3218, 2017.

Landry, J.-S., Matthews, H. D., and Ramankutty, N.: A global assessment of the carbon cycle and temperature responses to major changes in future fire regime, Climatic Change, 133, 179–192, 2015.

Latham, D. and Schlieter, J.: Ignition probabilities of wildland fuels based on simulated lightning discharges. Forest Service research paper, Tech. rep., Forest Service, Ogden, UT (USA). Intermountain Research Station, 1989.

Le Page, Y., Morton, D., Bond-Lamberty, B., Pereira, J., and Hurtt, G.: HESFIRE: a global fire model to explore the role of anthropogenic and weather drivers, Biogeosciences, 12, 887–903, 2015.

Levis, S., Bonan, G., Vertenstein, M., and Oleson, K.: The Community Land Model's dynamic global vegetation model (CLM-DGVM): Technical description and user's guide, NCAR Tech. Note TN-459+ IA, 50, 2004.

Li, F., Zeng, X., and Levis, S.: Corrigendum to" A process-based fire parameterization of intermediate complexity in a Dynamic Global Vegetation Model" published in Biogeosciences, 9, 2761–2780, 2012, Biogeosciences, 9, 4771–4772, 2012a.

Li, F., Zeng, X., and Levis, S.: A process-based fire parameterization of intermediate complexity in a Dynamic Global Vegetation Model, Biogeosciences, 9, 2761–2780, 2012b.

Li, F., Levis, S., and Ward, D.: Quantifying the role of fire in the Earth system–Part 1: Improved global fire modeling in the Community Earth System Model (CESM1), Biogeosciences, 10, 2293–2314, 2013.

https://doi.org/10.5194/egusphere-2022-961
Preprint. Discussion started: 1 November 2022

Li, F., Bond-Lamberty, B., and Levis, S.: Quantifying the role of fire in the Earth system–Part 2: Impact on the net carbon balance of global terrestrial ecosystems for the 20th century, Biogeosciences, 11, 1345–1360, 2014.

Matthews, H. D. and Caldeira, K.: Stabilizing climate requires near-zero emissions, Geophysical research letters, 35, 2008.

Matthews, H. D., Gillett, N. P., Stott, P. A., and Zickfeld, K.: The proportionality of global warming to cumulative carbon emissions, Nature, 459, 829–832, 2009.

Meissner, K., Weaver, A., Matthews, H., and Cox, P.: The role of land surface dynamics in glacial inception: a study with the UVic Earth System Model, Climate Dynamics, 21, 515–537, 2003.

Mengis, N., Keller, D. P., MacDougall, A. H., Eby, M., Wright, N., Meissner, K. J., Oschlies, A., Schmittner, A., MacIsaac, A. J., Matthews, H. D., et al.: Evaluation of the University of Victoria Earth System Climate Model version 2.10 (UVic ESCM 2.10), Geoscientific Model Development, 13, 4183–4204, 2020.

Moritz, M. A., Parisien, M.-A., Batllori, E., Krawchuk, M. A., Van Dorn, J., Ganz, D. J., and Hayhoe, K.: Climate change and disruptions to global fire activity, Ecosphere, 3, 1–22, 2012.

Olson, D. M., Dinerstein, E., Wikramanayake, E. D., Burgess, N. D., Powell, G. V., Underwood, E. C., D'amico, J. A., Itoua, I., Strand, H. E., Morrison, J. C., et al.: Terrestrial Ecoregions of the World: A New Map of Life on EarthA new global map of terrestrial ecoregions provides an innovative tool for conserving biodiversity, BioScience, 51, 933–938, 2001.

Pechony, O. and Shindell, D.: Fire parameterization on a global scale, Journal of Geophysical Research: Atmospheres, 114, 2009.

Pechony, O. and Shindell, D. T.: Driving forces of global wildfires over the past millennium and the forthcoming century, Proceedings of the National Academy of Sciences, 107, 19 167–19 170, 2010.

Pfeiffer, M., Spessa, A., and Kaplan, J. O.: A model for global biomass burning in preindustrial time: LPJ-LMfire (v1. 0), Geoscientific Model Development, 6, 643–685, 2013.

Prentice, S. and Mackerras, D.: The ratio of cloud to cloud-ground lightning flashes in thunderstorms, Journal of Applied Meteorology and Climatology, 16, 545–550, 1977.

Randerson, J., Chen, Y., Van Der Werf, G., Rogers, B., and Morton, D.: Global burned area and biomass burning emissions from small fires, Journal of Geophysical Research: Biogeosciences, 117, 2012.

Schneider, U., Becker, A., Finger, P., Meyer-Christoffer, A., Ziese, M., and Rudolf, B.: GPCC's new land surface precipitation climatology based on quality-controlled in situ data and its role in quantifying the global water cycle, Theoretical and Applied Climatology, 115, 15–40, 2014.

Spawn, S. A., Sullivan, C. C., Lark, T. J., and Gibbs, H. K.: Harmonized global maps of above and belowground biomass carbon density in the year 2010, Scientific Data, 7, 1–22, 2020.

Taylor, K. E.: Summarizing multiple aspects of model performance in a single diagram, Journal of Geophysical Research: Atmospheres, 106, 7183–7192, 2001.

Thonicke, K., Spessa, A., Prentice, I., Harrison, S. P., Dong, L., and Carmona-Moreno, C.: The influence of vegetation, fire spread and fire behaviour on biomass burning and trace gas emissions: results from a process-based model, Biogeosciences, 7, 1991–2011, 2010.

Tosca, M., Randerson, J., and Zender, C.: Global impact of smoke aerosols from landscape fires on climate and the Hadley circulation, Atmospheric Chemistry and Physics, 13, 5227–5241, 2013.

van der Werf, G. R., Randerson, J. T., Giglio, L., Collatz, G. J., Kasibhatla, P. S., and Arellano Jr, A. F.: Interannual variability in global biomass burning emissions from 1997 to 2004, Atmospheric Chemistry and Physics, 6, 3423–3441, 2006.

https://doi.org/10.5194/egusphere-2022-961
Preprint. Discussion started: 1 November 2022

Van der Werf, G. R., Randerson, J. T., Giglio, L., Collatz, G., Mu, M., Kasibhatla, P. S., Morton, D. C., DeFries, R., Jin, Y. v., and van Leeuwen, T. T.: Global fire emissions and the contribution of deforestation, savanna, forest, agricultural, and peat fires (1997–2009), Atmospheric chemistry and physics, 10, 11 707–11 735, 2010.

Venevsky, S., Thonicke, K., Sitch, S., and Cramer, W.: Simulating fire regimes in human-dominated ecosystems: Iberian Peninsula case study, Global Change Biology, 8, 984–998, 2002.

Voinov, A. and Shugart, H. H.: 'Integronsters', integral and integrated modeling, Environmental Modelling & Software, 39, 149–158, 2013.

Ward, D., Kloster, S., Mahowald, N., Rogers, B., Randerson, J., and Hess, P.: The changing radiative forcing of fires: global model estimates for past, present and future, Atmospheric Chemistry and Physics, 12, 10 857–10 886, 2012.

Weaver, A. J., Eby, M., Wiebe, E. C., Bitz, C. M., Duffy, P. B., Ewen, T. L., Fanning, A. F., Holland, M. M., MacFadyen, A., Matthews, H. D., et al.: The UVic Earth System Climate Model: Model description, climatology, and applications to past, present and future climates, Atmosphere-Ocean, 39, 361–428, 2001.

Wu, C., Venevsky, S., Sitch, S., Mercado, L. M., Huntingford, C., and Staver, A. C.: Historical and future global burned area with changing climate and human demography, One Earth, 4, 517–530, 2021.

Yang, J., Tian, H., Tao, B., Ren, W., Lu, C., Pan, S., Wang, Y., and Liu, Y.: Century-scale patterns and trends of global pyrogenic carbon emissions and fire influences on terrestrial carbon balance, Global Biogeochemical Cycles, 29, 1549–1566, 2015.

Yue, C., Ciais, P., Cadule, P., Thonicke, K., Archibald, S., Poulter, B., Hao, W., Hantson, S., Mouillot, F., Friedlingstein, P., et al.: Modelling the role of fires in the terrestrial carbon balance by incorporating SPITFIRE into the global vegetation model ORCHIDEE–Part 1: simulating historical global burned area and fire regimes, Geoscientific Model Development, 7, 2747–2767, 2014.

Zelazowski, P., Huntingford, C., Mercado, L. M., and Schaller, N.: Climate pattern-scaling set for an ensemble of 22 GCMs–adding uncertainty to the IMOGEN version 2.0 impact system, Geoscientific Model Development, 11, 541–560, 2018.

Zickfeld, K., Eby, M., Matthews, H. D., and Weaver, A. J.: Setting cumulative emissions targets to reduce the risk of dangerous climate change, Proceedings of the National Academy of Sciences, 106, 16 129–16 134, 2009.